ANTENNA PATTERN CONTROL USING IMPEDANCE SURFACES

GRANT
IN-32-CR
39564
p28

Semiannual Progress Report

Constantine A. Balanis and Kefeng Liu

March 16, 1991 - September 15, 1991

Telecommunication Research Center
Department of Electrical Engineering
Arizona State University
Tempe, Arizona 85287-7206

Grant No. NAG-1-1183
National Aeronautics and Space Administration
AVRADA Joint Research Program Office
Langley Research Center
Hampton, VA 23665

ANTENNA PATTERN CONTROL USING IMPEDANCE SURFACES

Semiannual Progress Report

Constantine A. Balanis and Kefeng Liu

March 16, 1991 - September 15, 1991

Telecommunication Research Center
Department of Electrical Engineering
Arizona State University
Tempe, Arizona 85287-7206

Grant No. NAG-1-1183
National Aeronautics and Space Administration
AVRADA Joint Research Program Office
Langley Research Center
Hampton, VA 23665

ABSTRACT

This is a semiannual progress report for the *Antenna Pattern Control Using Impedance Surfaces* research grant. This report covers the research period from March 16, 1991 to September 15, 1991.

During this research period, the implementation of a moment method code for the analysis of horn antennas has been accomplished. The code can analyze the antenna with or without lossy material coatings. It predicts the antenna gain, VSWR on the feeding waveguide, the existing modes on the radiating aperture, and radiation patterns of the antenna. Many computations have been performed on three pyramidal horn antennas, and their radiation patterns and VSWR's are presented and compared to experimental data. While the code is still being finalized, some discussions in using the code are included. After the analysis code is completed, we will move to the synthesis problem in the coming research period.

I. INTRODUCTION

As a continuation of last research period, we have been concentrating our efforts on the implementations of the methods presented on the previous report. The major obstacle during this research period has been the computer memory needed for the code. At the beginning of this research period, the implementation of the moment method and stepped waveguide techniques for the analysis of the horn antennas of perfectly conducting surfaces was accomplished. The approximate core memories required are, respectively, 30 megawords (240 Mbytes) for the 20-dB standard gain horn, 50 megawords for the 5-inch square horn, and 100 megawords for the 7-in square horn. At first, a few testing cases of the X-band standard gain horn were run in the Cray Y-MP/464 and Cray-2 computers of National Center for Supercomputer Applications (NCSA). Good results were obtained for the standard X-band horn. However, some problems were encountered for larger horns. Further usages of the NCSA computing facilities proved to be a very inconvenient task.

An alternative out-of-core memory matrix solver was investigated to allow the computations to be performed under Arizona State University's Cray X-MP/18se (now X-MP/116se). The available out-of-core matrix solver in the Bench Library of the Cray Research Incorporation is the one that solves full square matrix system equations. Since the moment method problem we formulated uses the Galerkin's testing procedure, the impedance matrix is symmetrical. Therefore, only the upper or the lower portions of the impedance elements need to be computed and stored. Moreover, the impedance elements on the aperture have a Toeplitz property that is utilized to save the computation time dramatically. While Toeplitz and symmetrical properties are good features for CPU saving, they become difficult features for us to

use in the full system equations solver because it is very time consuming to locate and retrieve the computed moment method impedance elements which were previously stored in the peripheral storage device. The other disadvantage in using the full matrix out-of-core solver is that it requires almost twice the peripheral storage and twice the matrix LU decomposition time as that of the symmetrical system.

Inspired by the techniques in a presentation on reducing the memory thrashing for the full matrix solver in Virtual Machine System (VMS) by Dr. Burton [1] in 1991 Symposium on Antennas and Propagations in London, Ontario, Canada, we decided to develop a symmetrical system solver of our own. With the help of the Arizona State University supercomputer consultants Mr. Dale Wultz and Bruce Tachoir on the fast buffer I/O's of the UNICOS system, we have successfully developed an efficient out-of-core memory solver for symmetrical complex matrix. A comprehensive testing of our symmetrical solver has demonstrated that the solver is stable, accurate, and just about as efficient as that of the in-core solver. The computer code was then modified into a version which uses the out-of-core matrix solver in the moment method solution. The computed results and discussions in modeling the pyramidal horn antennas using the code are presented in the next section.

II. RESULTS

The computer code for the analysis of pyramidal horn antennas is based on the moment method and stepped waveguide techniques presented in the previous report. The code uses a stepped waveguide technique to analyze the continuous horn transition in the interior of the horn antenna, and an integral equation formulation to analyze the radiation and scattering of the radiating aperture and the outer surfaces of

the horn. The hybrid field integral equations were solved by using the moment method with roof-top subsection base function and Galerkin's testing. To accurately account for the rippling effects of the radiation pattern in the back side of the radiation pattern, the entire outer surface of the horn antenna is included in the integral equation and moment method solution.

Although the code is also designed to analyze the pyramidal horn antennas with lossy material walls, they have not been extensively tested yet. Therefore, the results for lossy material coatings are not presented in this report. Like any other numerical electromagnetic code, the accuracy of the computed results from the code we developed can be affected by:

- The segment size of the subsectional roof-top base and testing functions in the integral equation and moment method analysis of radiating aperture and the exterior surfaces of the horn antenna.

- The step size of the stepped-waveguide and the total number of waveguide modes included in the stepped-waveguide technique in analyzing the wave transition in the interior region of the horn.

The importance of these factors in the accuracy of the computation results will be discussed for the three pyramidal horn antennas that we have analyzed.

A. Modeling the X-band Standard gain horn

Computations were first performed to analyze an X-band horn. The 20-dB X-band standard gain horn has dimensions of 4.87 inches by 3.62 inches on the aperture, and 10.06 inches in length. The analyses were carried out at 10 GHz, and 10.1 GHz respectively, and the results were compared with experimental data. Table 1 lists

typical computational requirements for the moment method code to perform in-core analysis of the X-band standard gain horn operating at 10 GHz and 10.1 GHz.

Table 1: Typical Computation Requirements for the X-band Horn

	At 10 GHz	At 10.1 GHz
Maximum Step Size	$\frac{\lambda}{16}$	$\frac{\lambda}{16}$
Waveguide Modes	90	90
Maximum Segment Size	0.1875λ	0.1875λ
Number of Elements	5082	5573
Core Memory (in Mws)	30	34
CPU (in seconds)	4035.6 (in Y-MP)	4114.5 (in Cray-2)

Comparisons of the computed and measured antenna gains and VSWR's in the feeding adaptor are listed in Table 2.

Table 2: Antenna Parameters for X-band Horn Antennas

	At 10 GHz		At 10.1 GHz	
	Computed	Experiment	Computed	Experiment
Gain (in dB's)	20.63	20.46	20.69	20.54
VSWR	1.057	1.06	1.051	1.05

Figures 1 and 2 show the comparison between the computed and experimental E- and H-plane radiation patterns of the antennas. The two figures were obtained from the in-core version of the codes computed using the Y-MP/464 of the NCSA. Good agreements between the computed and the measured radiation patterns can be observed from the two figures presented. In the back regions of the H-plane pattern, some discrepancies in the ripple structure are also observed. We believe these discrepancies are contributed by:

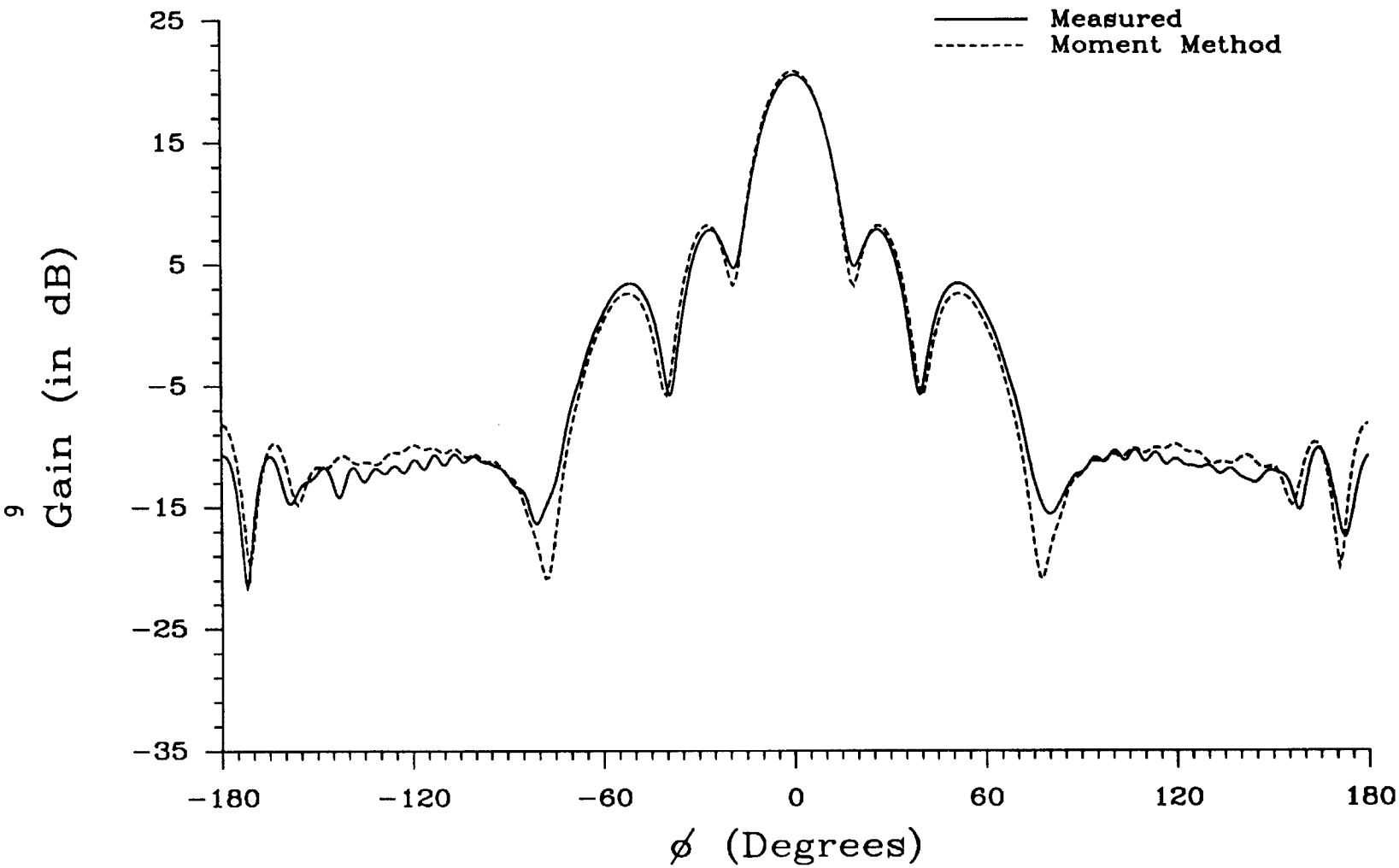

Figure 1. Comparison of E−plane radiation patterns for an X−band standard gain horn at 10 GHz.

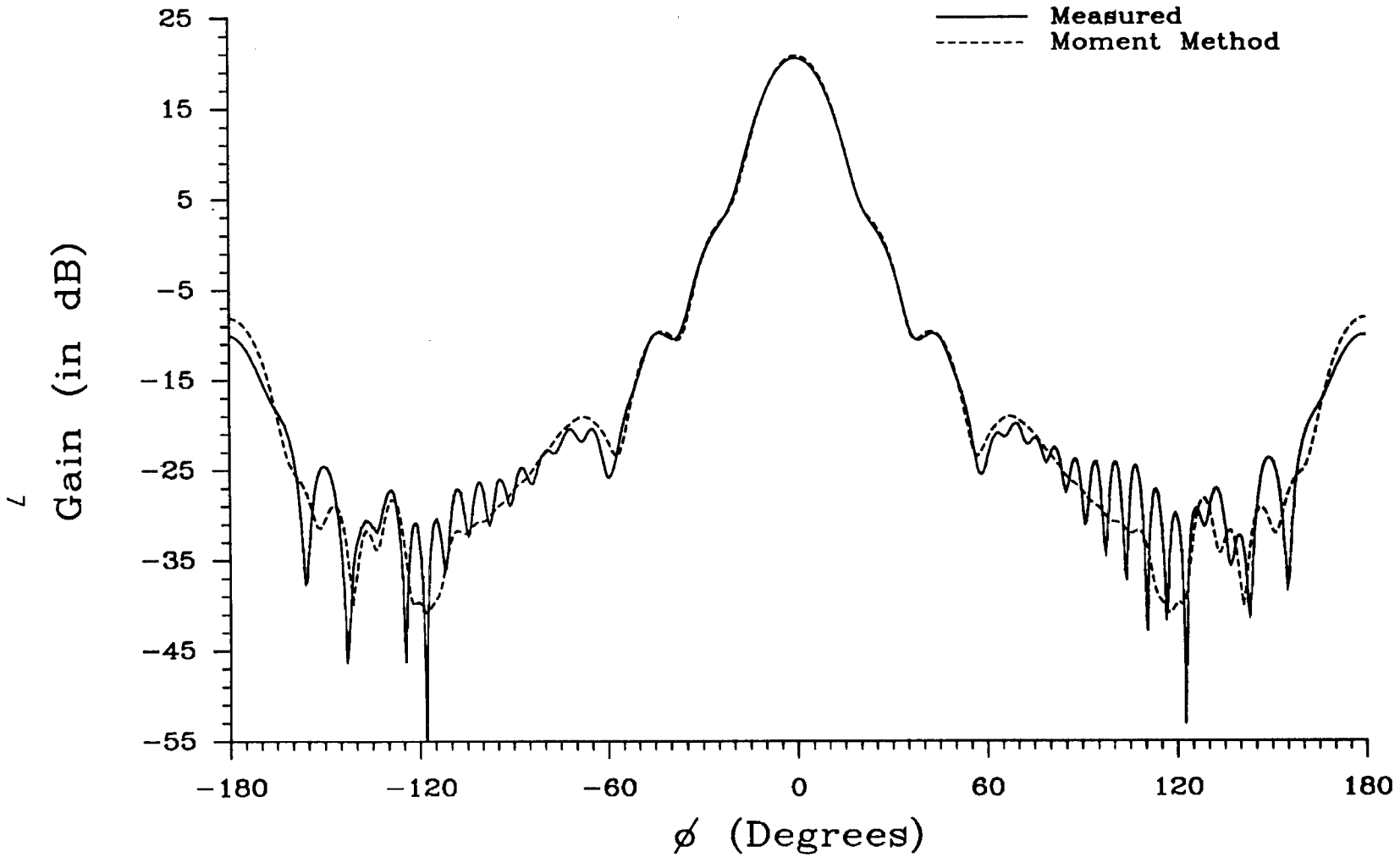

Figure 2. Comparison of H−plane radiation patterns for a standard X−band gain horn at 10 GHz.

- The segment size of the subsectional roof-top base and testing functions as outlined previously.

- The cable and the outer surfaces of the feeding waveguide adaptor which the code did not model. We observed some discrepancies in the rapid ripple structures between two measured H-plane radiation patterns due to different layouts of the feeding cable. Discrepancies are also contributed by a minor asymmetry of the antenna. Some slightly asymmetrical ripple structures can be observed from the measured H-plane radiation patterns in Figure 2 and other figures presented in this report.

To demonstrate the accuracy and the efficiency of the out-of-core matrix solver, the same case was also computed using the Cray X-MP/18se at Arizona State University with the out-of-core version of the moment method code. As expected, identical radiation patterns and other key antenna parameters were obtained. A comparison of computation requirements between the two versions of the computer code is shown in Table 3.

Table 3: Computation Comparison Between the In-core and Out-of-core codes

	Y-MP/464 (NCSA)	X-MP/18se (ASU)
Number of Elements	5082	5082
Core Memory (in Mws)	30	5
Peripheral Storage		197 Mbytes
CPU (in seconds)	4035.6	5388.4

We would like to point out that a part of the CPU difference in Table 3 is contributed by the performances of the two different Cray machines. Therefore, as pre-

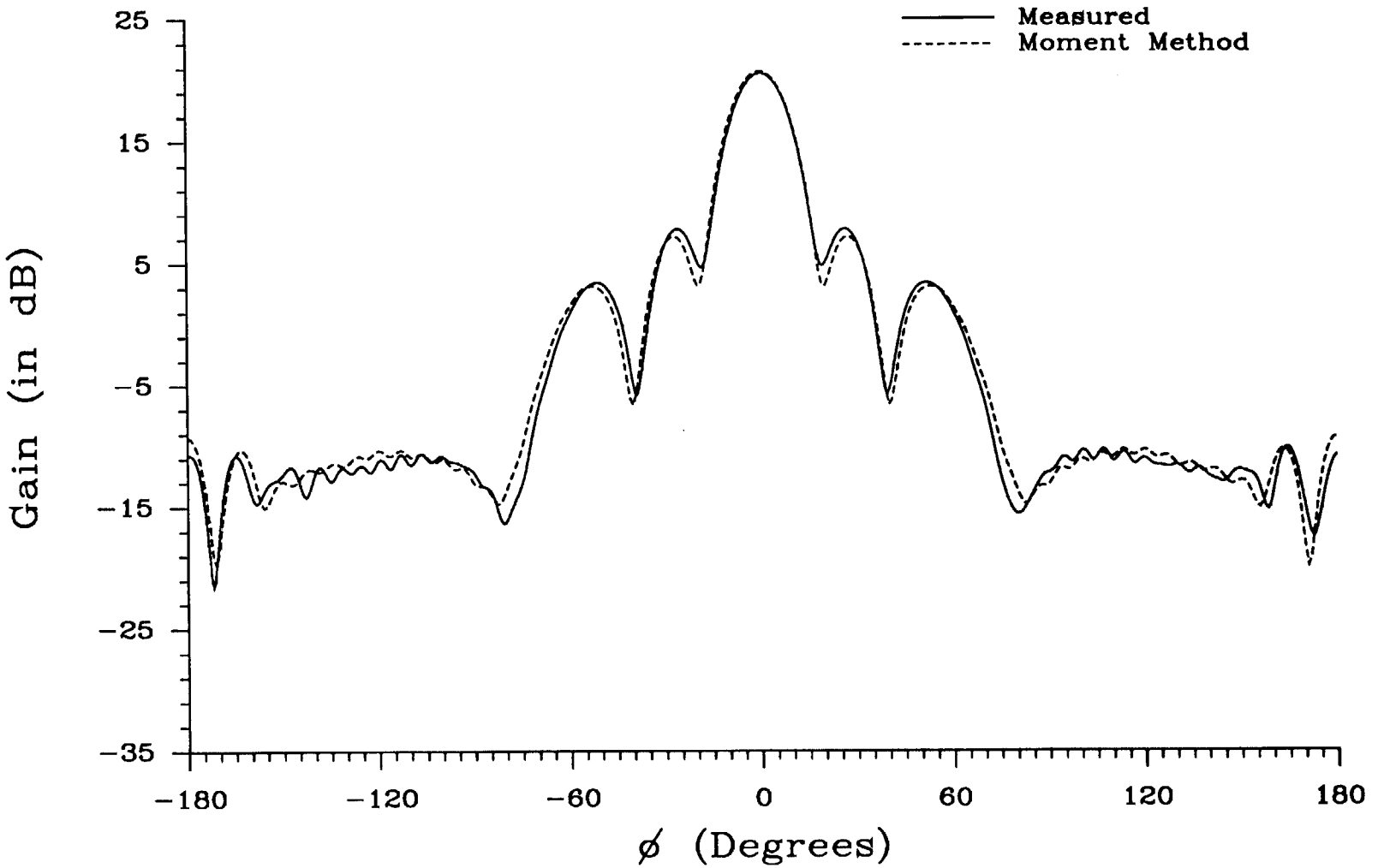

Figure 3. Comparison of E−plane radiation pattern for an X−band standard gain horn at 10. GHz. Smaller step and segment sizes are used in this case.

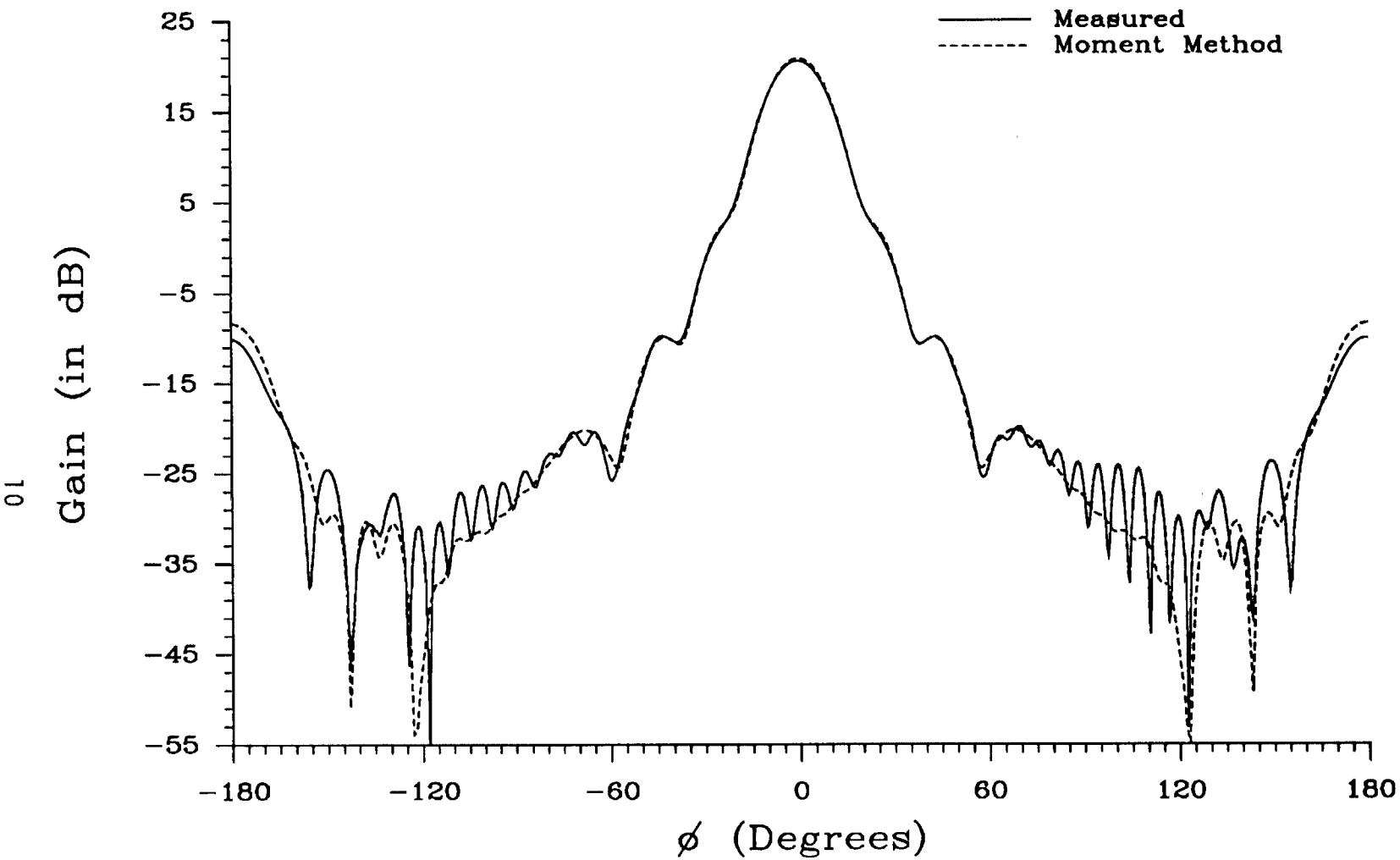

Figure 4. Comparison of H-plane radiation pattern for an X-band standard gain horn at 10. GHz. Smaller step and segment sizes are used in this case.

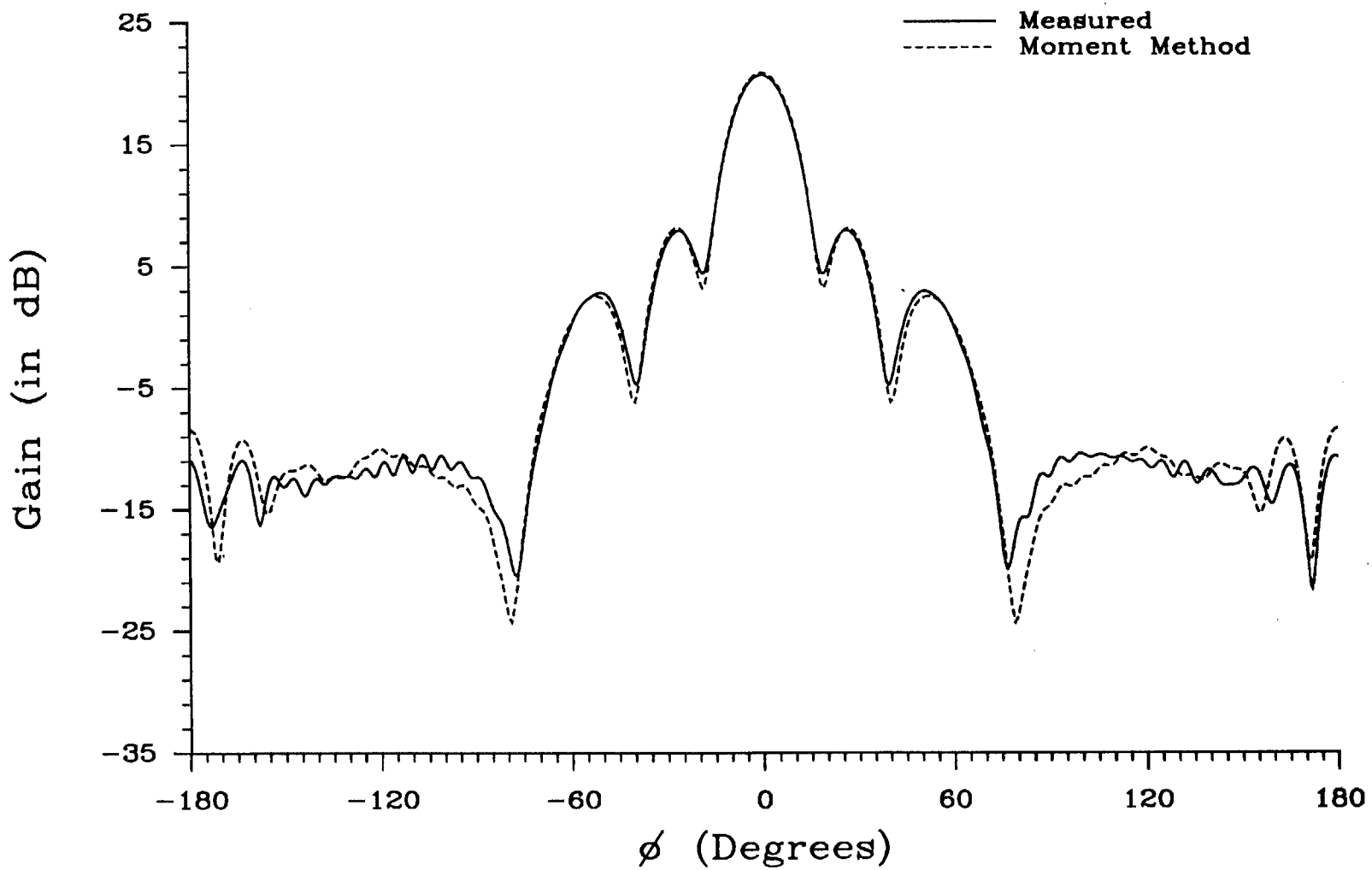

Figure 5. Comparison of E−plane radiation patterns for an X−band standard gain horn at 10.1 GHz.

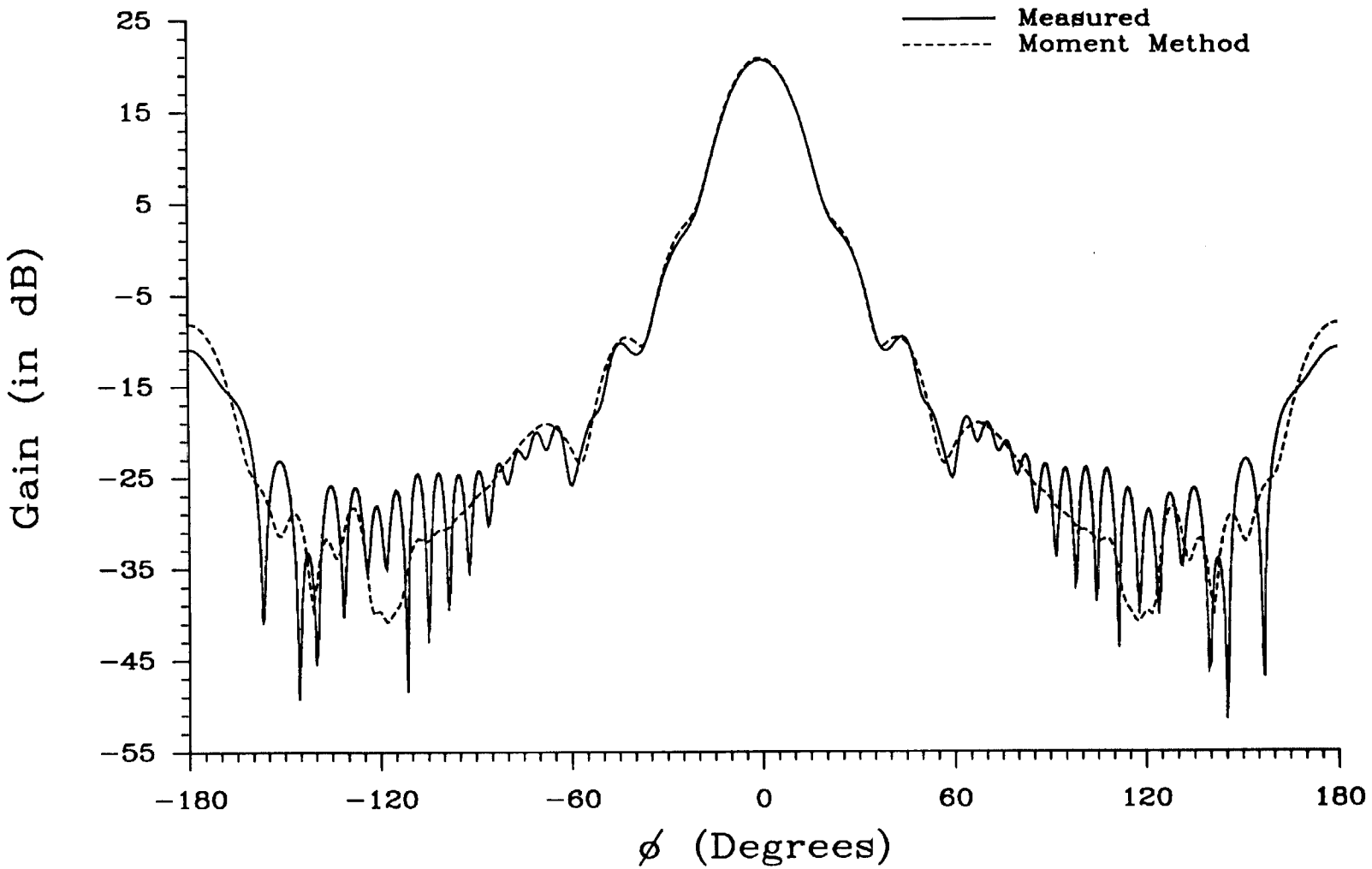

Figure 6. Comparison of H−plane radiation patterns for an X−band standard gain horn at 10.1 GHz.

sented in Table 3, the comparison demonstrates an excellent efficiency of the out-of-core matrix solver under the UNICOS system.

To test the robustness and the accuracy of the computer code, a smaller segment size of 0.15λ and a smaller step waveguide size of $\frac{\lambda}{32}$ were introduced into the computations of X-band horn at 10 GHz using the out-of-core version of the code. Figures 3 and 4 represent, respectively, computed E- and H-plane radiation patterns as compared to the measured patterns in Figures 1 and 2. As expected, a significant improvement in the agreement between the computed and measured patterns is observed from both figures. The H-plane pattern starts to exhibit some of the rapid ripple structures. Further improvements in the rapid ripple structures of the H-plane pattern can be expected by using smaller segment size. However, the price for such an improvement is a very significant increase in computation.

Figures 5 and 6 represent the comparisons of the E- and H-plane radiation patterns at 10.1 GHz. The parameters used in computing these two patterns have already been listed in Table 1. As expected, the code demonstrates about the same order of accuracy as the results at 10 GHz.

B. Modeling the Square Aperture Horns

Computational analyses of two square aperture horns were also performed and compared with the experiments. The smaller horn has dimensions of 5.04 inches by 5.06 inches on the aperture, and 10.5 inches in length (5-in horn). The larger one has 6.98 inches by 7.00 inches on the aperture, and 12.2 inches in length (7-in horn). The electrical sizes of these two horn are much larger than the X-band standard gain horn presented previously. They are much more time consuming in performing the analysis. Table 4 outlines some typical computation figures in running the code.

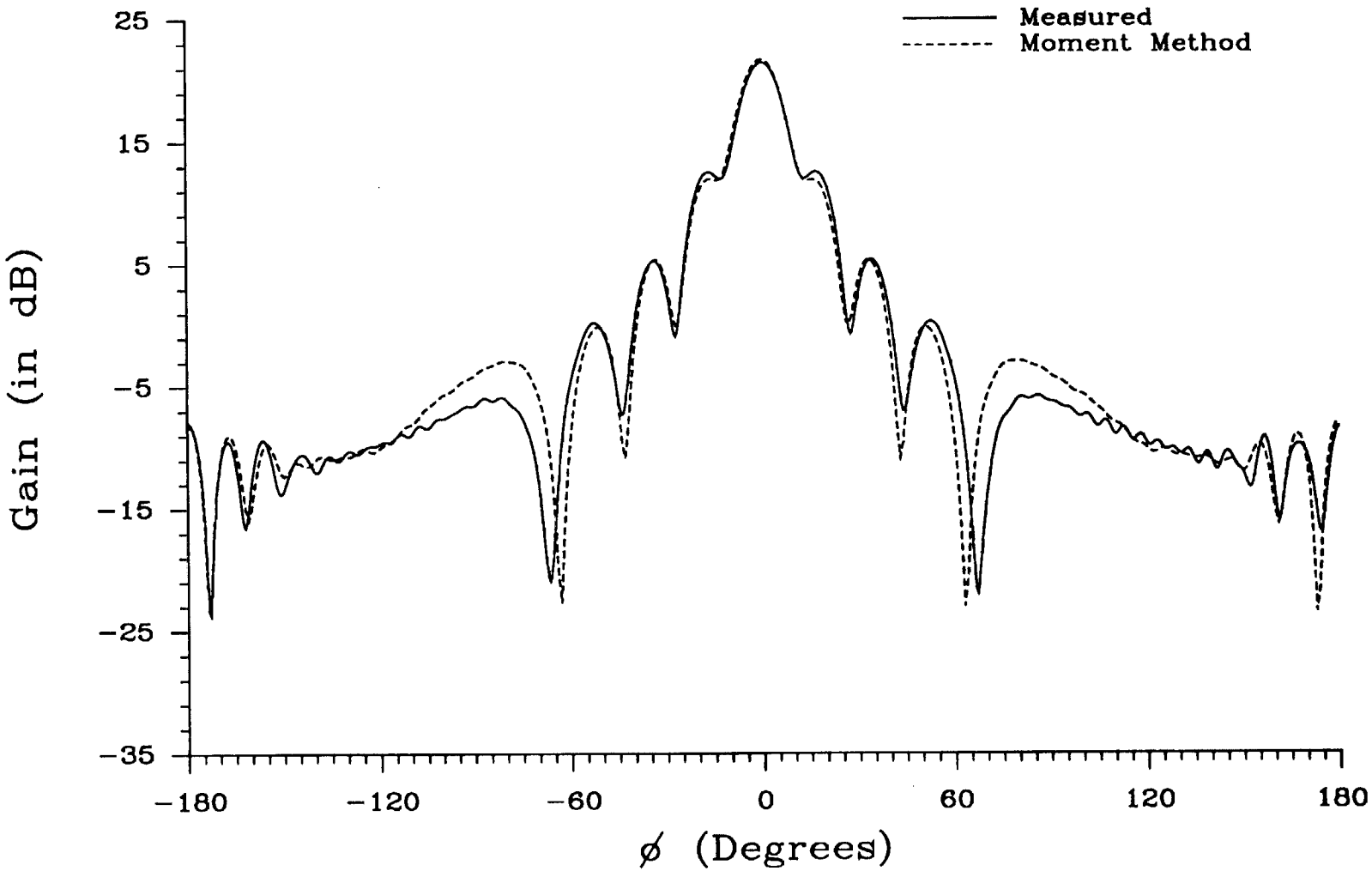

Figure 7. Comparison of E-plane radiation patterns for a 5"X5" square aperture horn at 10 GHz.

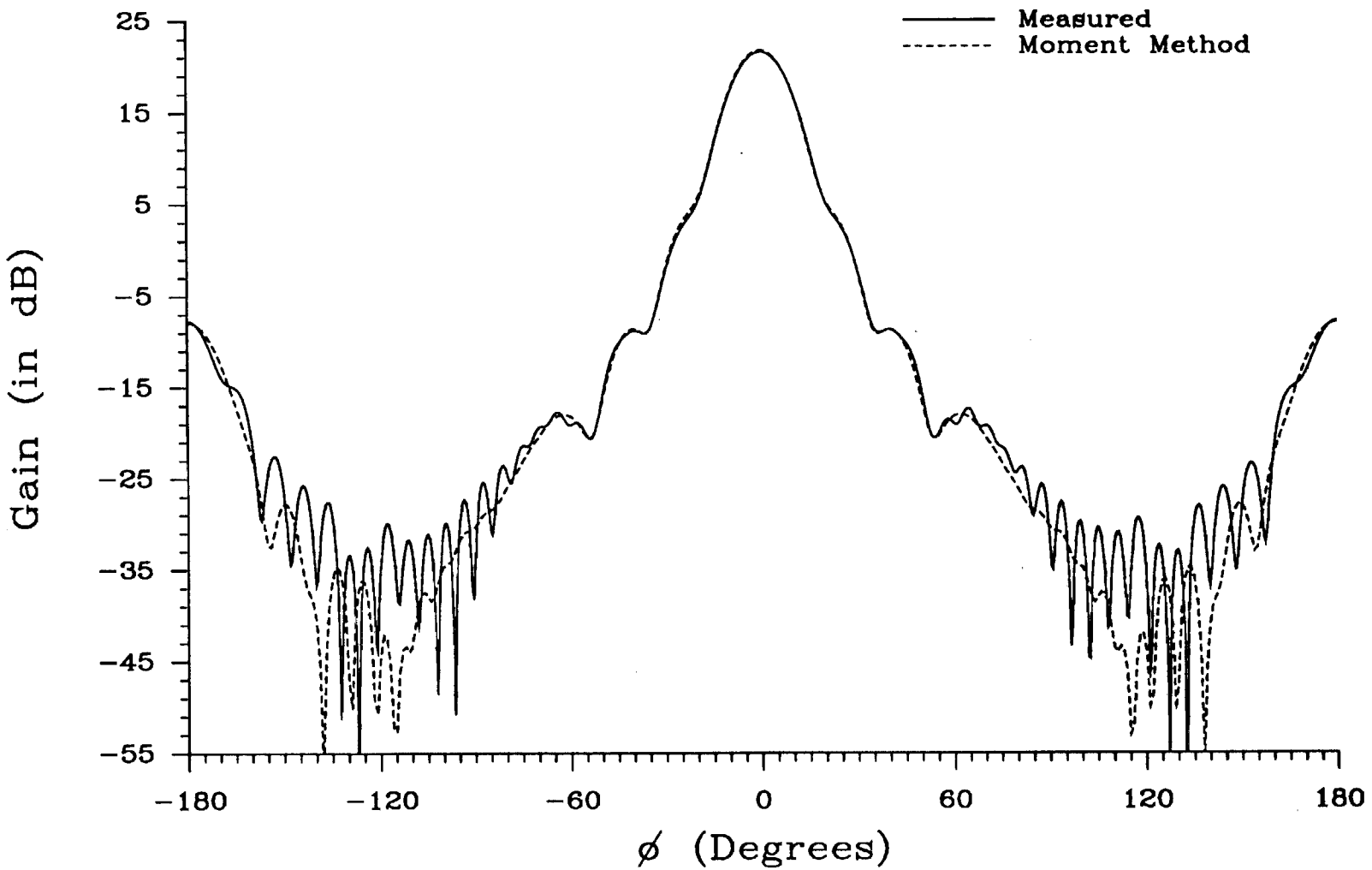

Figure 8. Comparison of H-plane radiation patterns for a 5"X5" square aperture horn at 10 GHz.

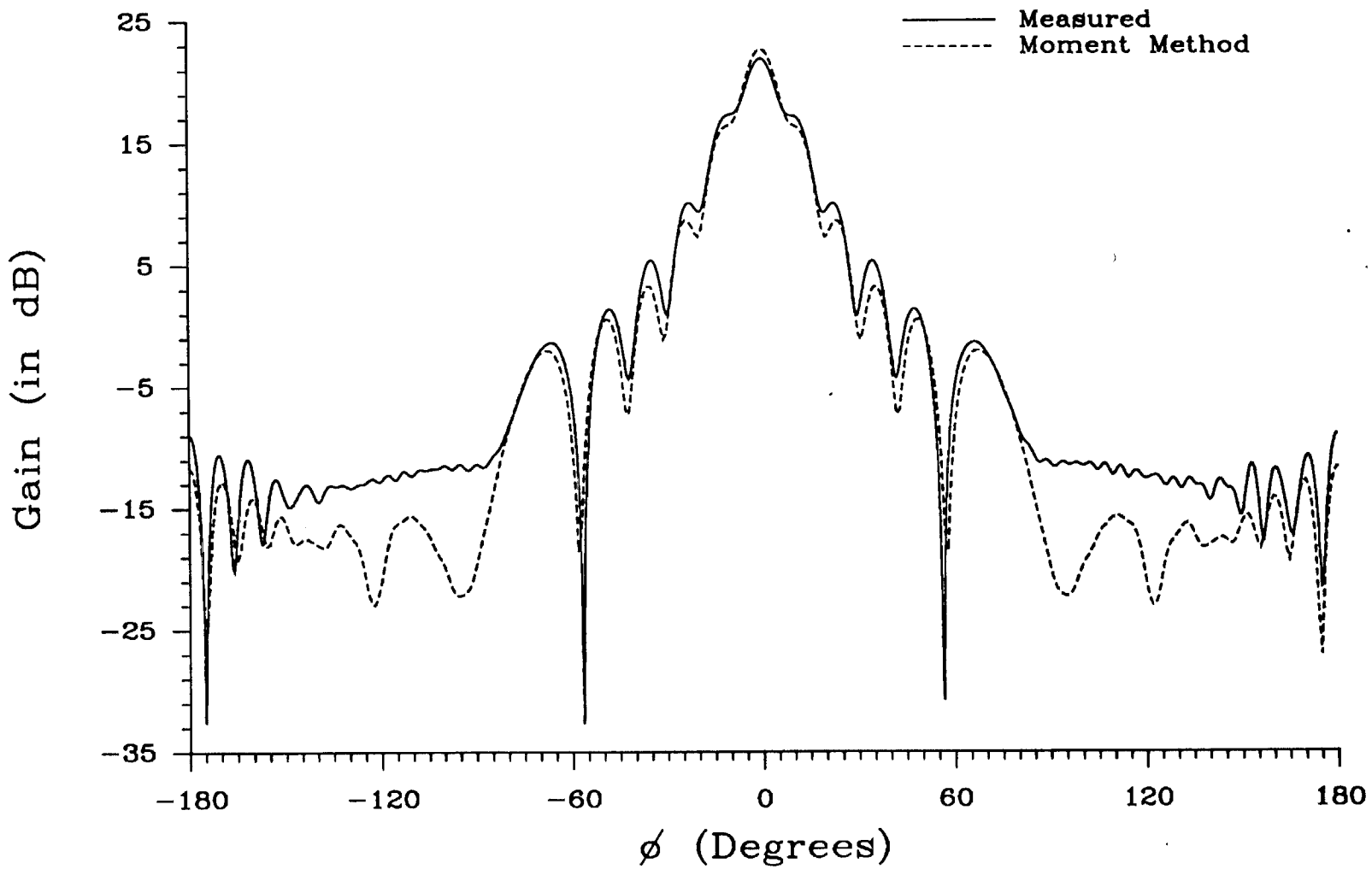

Figure 9. Comparison of E-plane radiation patterns for a 7"X7" square aperture horn at 10 GHz.

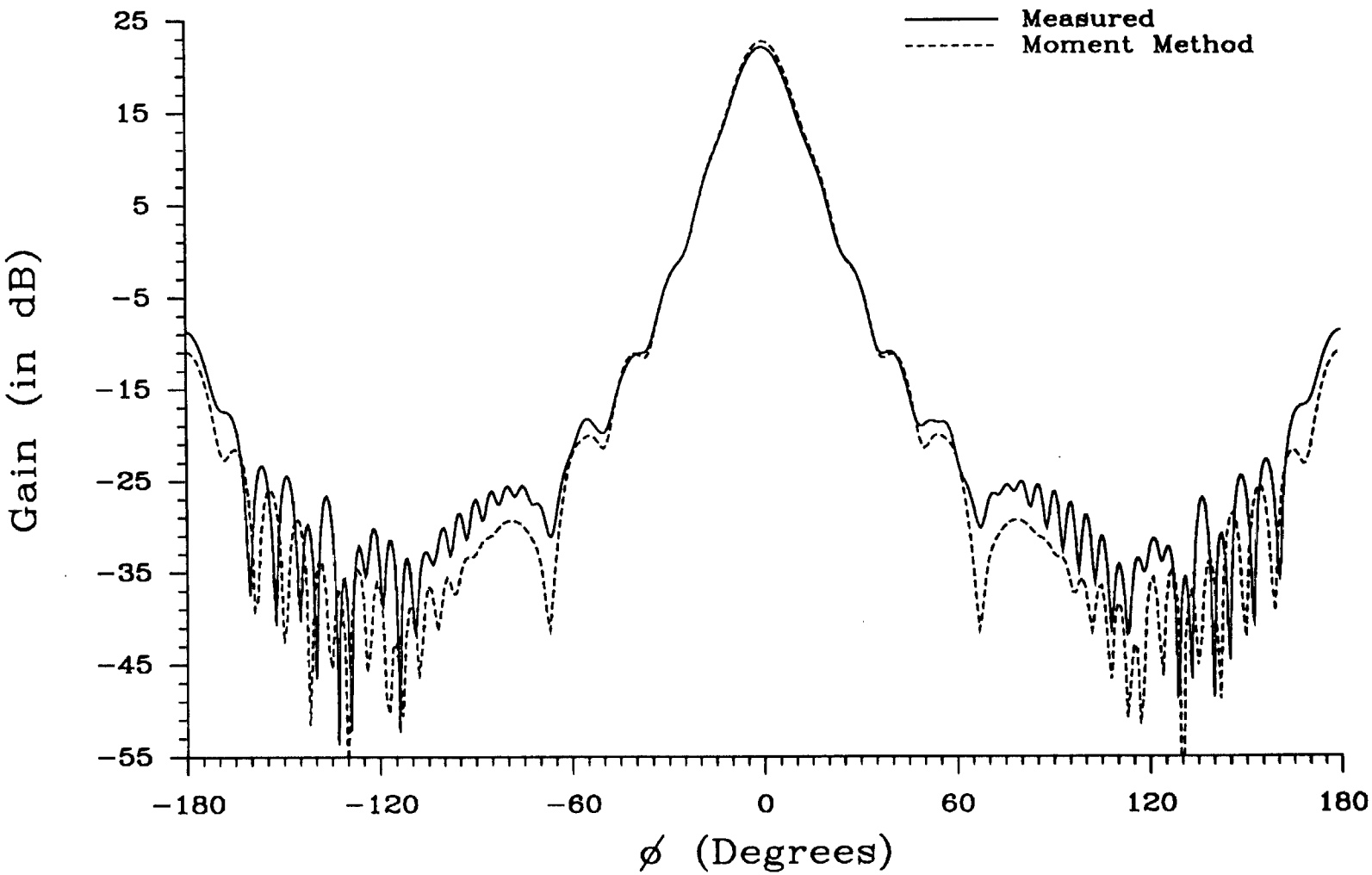

Figure 10. Comparison of H-plane radiation patterns for a 7"X7" square aperture horn at 10 GHz.

Table 4: Computation Figures to analyze the Two Square Horns

	5-in Horn	7-in Horn
Maximum Step Size	$\frac{\lambda}{32}$	$\frac{\lambda}{16}$
Waveguide Modes	90	90
Maximum Segment Size	0.1875λ	0.1875λ
Number of Elements	7324	9946
Core Memory (in Mws)	10	10
Peripheral Storage	430 Mbytes	800 Mbytes
CPU (in hours)	3.8	6.8
Turn-Around Time	5 days	8 days or more

Figures 7 and 8 exhibit the computed E- and H-plane radiation patterns which are compared to those measured patterns for the 5-in horn. Figures 9 and 10 represent for the 7-in horn. As we observe from the figures, the computed patterns do not agree with the experimental patterns very well in some regions. We strongly suspect that the larger flaring angles in the horns are the main sources of inaccuracy in the computed radiation patterns. Our computed results have shown that the higher order modes on the radiating apertures of the two square aperture horns have much larger values than those of the X-band standard gain horn. The more important presence of the higher order modes is a direct result of a horn with a large flaring angle. Therefore, more waveguide modes and finer step size are required to accurately account for the interior horn transitions. One confirmation of the assumption is that a better agreement of E-plane radiation patterns, which are presented in Figure 7, have been found when we reduce the stepped waveguide size from $\frac{\lambda}{16}$ to $\frac{\lambda}{32}$. In the next reporting period, we will attempt to resolve the discrepancy between the computations and the measurements by optimizing the code to include more waveguide modes while maintaining an efficient size of the core memory required in the out-of-core solver.

C. Horn Antennas Mounted on a Ground Plane

In this research period, another version of moment method code was also developed to analyze pyramidal horn antennas mounted on an infinite ground plane. This development will enable us to have the capability to model the horn antenna mounted on a large conducting body. The presence of the ground plane greatly simplifies the integral equation and moment method procedure because only the magnetic field integral equation on the radiating aperture is needed to analyze such an antenna. The outer surfaces of the antenna do not need to be modelled because they are shielded by the infinite ground plane. The only time consuming part of the analysis is the stepped waveguide analysis for the interior horn transition, which is a fraction of the total CPU needed in the analysis of the same antenna without the ground plane.

The experimental model of the infinite ground plane was a difficult task in the past. Recently, a very simple technique to experimentally model an infinite ground plane using a finite ground plane was introduced by Williams in [2]. The technique utilizes the property of the first order diffracted fields from the edges of the finite ground plane, and uses the measured radiation pattern in the back-side of the finite ground plane to correct the front-side of the radiation patterns. Therefore, the corrected front side radiation patterns accurately represent the radiation patterns of the antenna as if it were mounted on an infinite ground plane. While long turn-around-time moment method computations were queuing for number crunching, we decided to develop this measurement capacity using such a simple technique. After some considerations of the quiet-zone limits and the time gating limits in eliminating the multiple scattering, a 3 feet by 3 feet planar aluminum sheet was used to emulate the ground plane. Again, the X-band standard gain horn was first mounted on the

ground plane. Figures 11 and 12 show the comparison of the measured and the computed E- and H-plane radiation patterns. Since the mounted ground plane is large electrically and it emulates well the infinite ground plane, the uncorrected experimental data already agree with the theoretical predictions very well except at the region near the edges. The measured data were processed to translate the rotation center of the antenna from experimental setup into aperture center. Techniques in eliminating the diffracted fields due to the edges of the finite ground plane presented in [2] were applied. Figures 13 and 14 represent, respectively, the E- and H-plane radiation patterns of the treated experimental data compared to the computed patterns. They clearly show that the diffracted fields are almost eliminated. As a result, a much better agreement between the theoretical prediction and the experimental pattern on the edges is obtained.

III. FUTURE WORK

In the coming research period, research will be focused on the accurate modeling of the horn antennas with material coating. When such a modeling is completed, the synthesis techniques are going to be implemented and compared with the experiments.

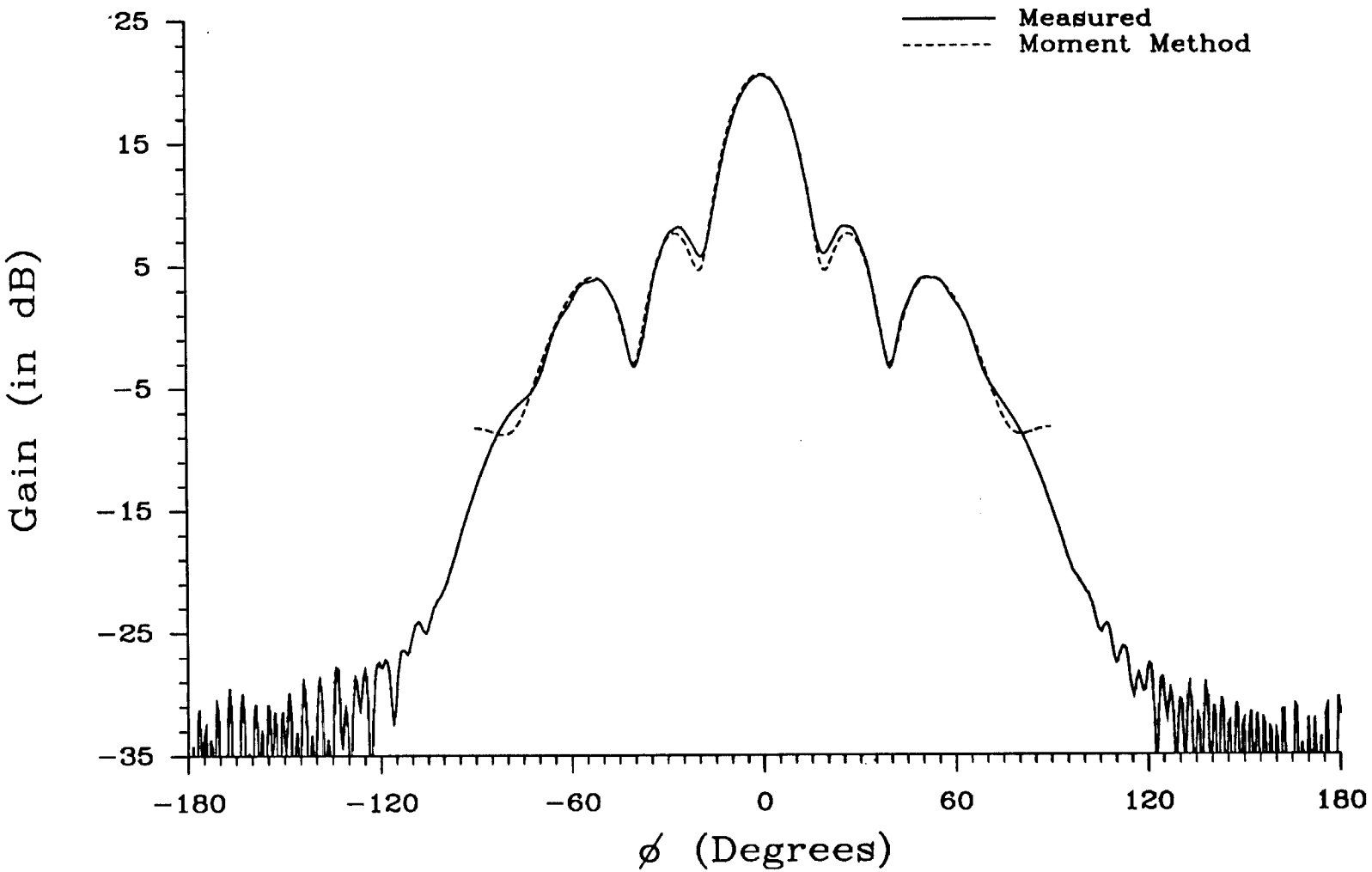

Figure 11. E−plane radiation patterns of the X−band standard gain horn mounted on a 3'X3' ground plane. The measured pattern includes diffracted fields from the edges.

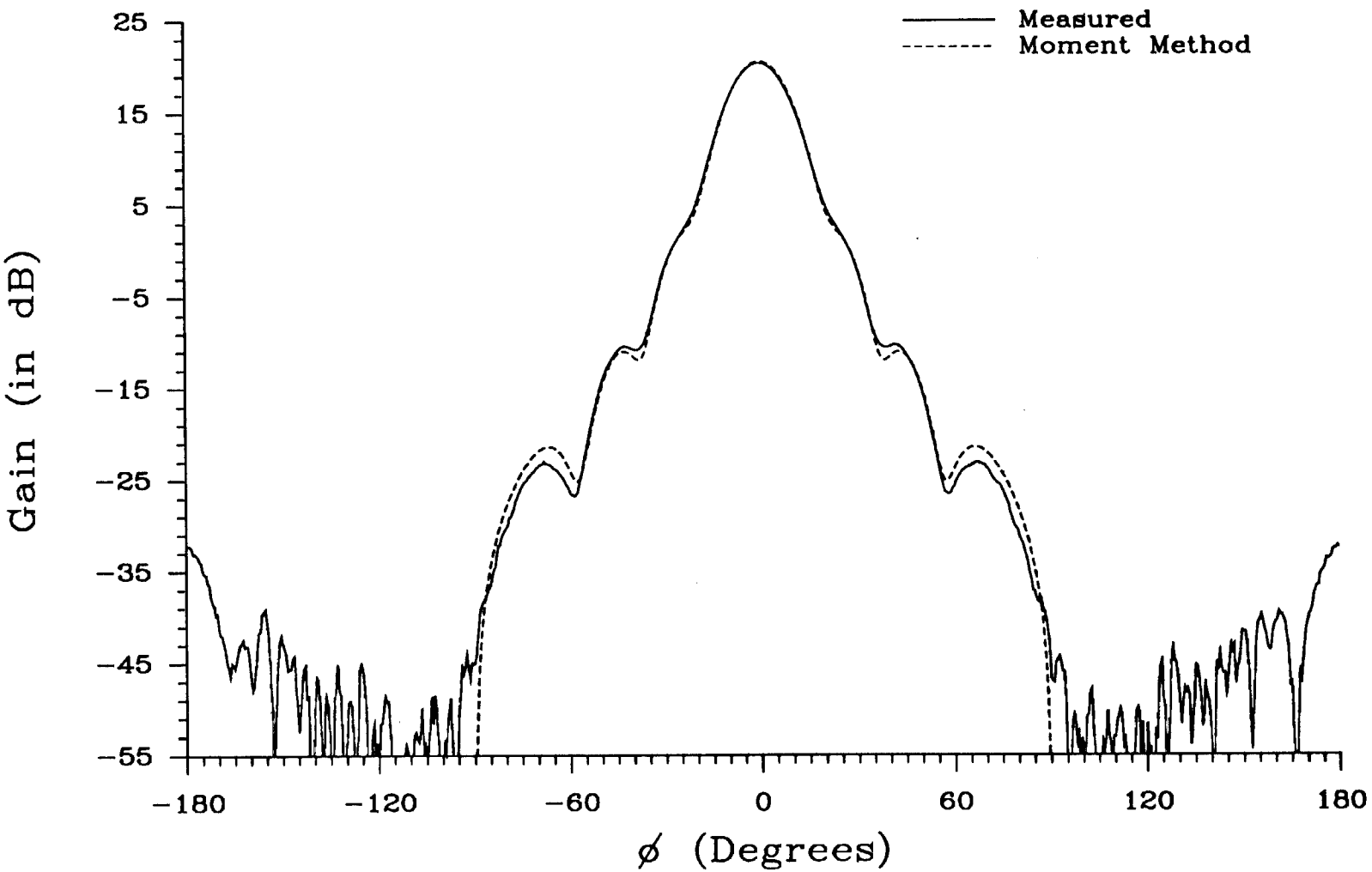

Figure 12. H-plane radiation patterns of the X-band standard gain horn mounted on a 3'X3' ground plane. The measured pattern includes diffracted fields from the edges.

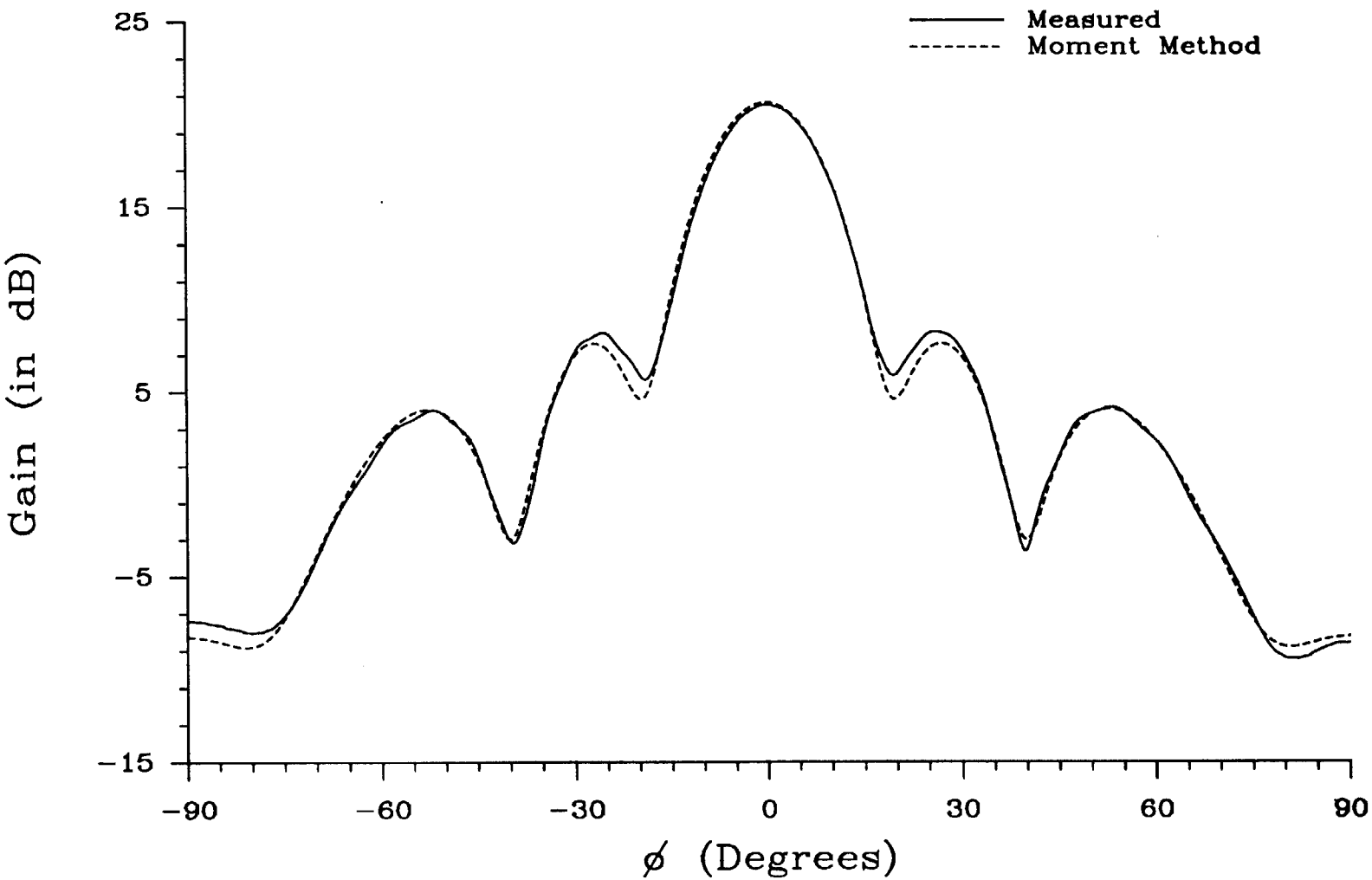

Figure 13. E−plane radiation patterns of the X−band standard gain horn mounted on a 3'X3' ground plane. The diffracted fields have been corrected in the measured pattern.

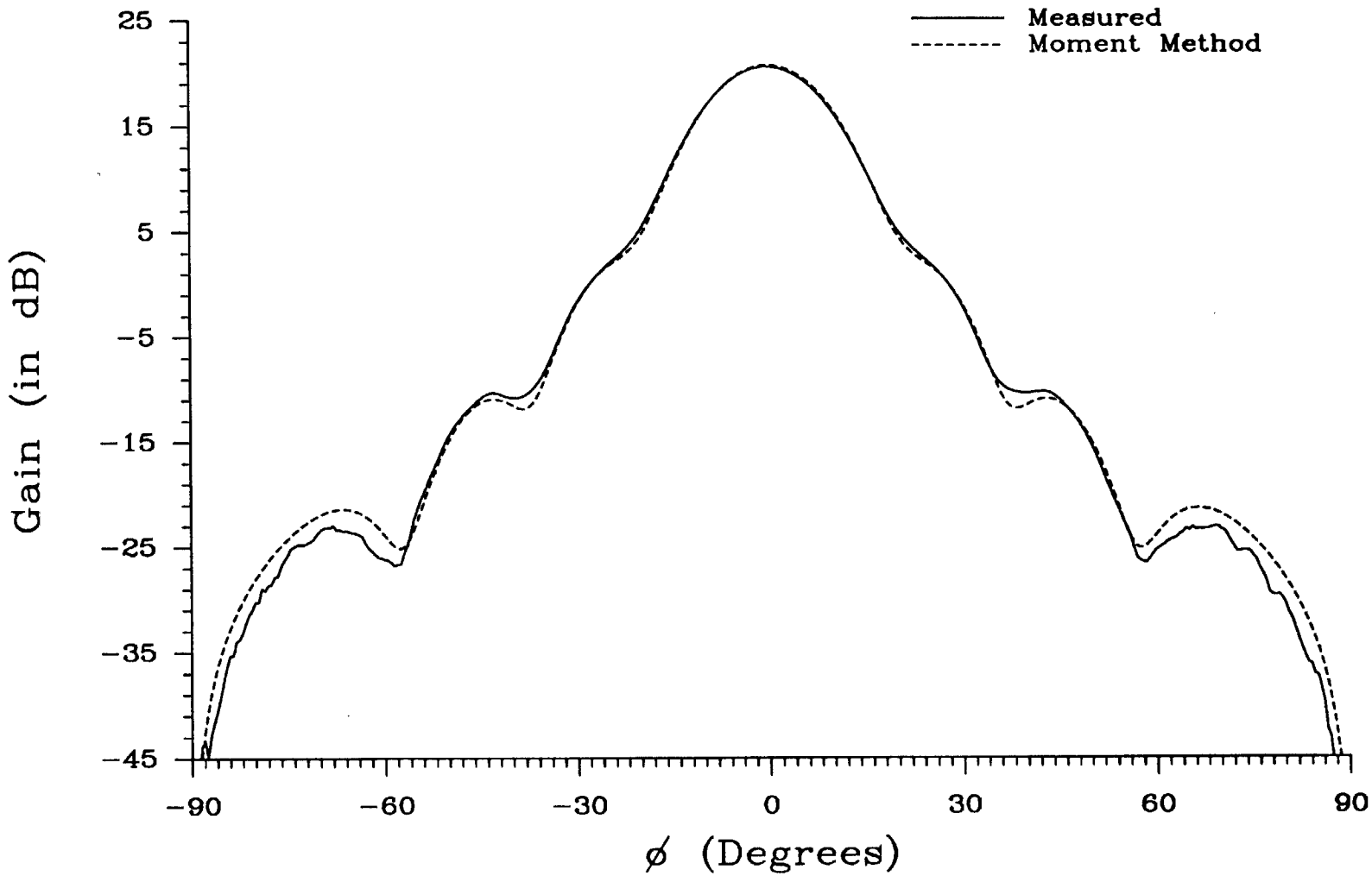

Figure 14. H-plane radiation patterns of the X-band standard gain horn mounted on a 3'X3' ground plane. The diffracted fields have been corrected in the measured pattern.

IV. PUBLICATIONS

During this reporting period, two papers have been published in the IEEE Transaction on Antennas and Propagations. One paper was presented in an international symposium. The papers published or presented are all under the sponsorship of the NASA-AVRADA Joint Research Program Research Program Office research grant No. NAG-1-1183.

1. Kefeng Liu and C. A. Balanis, "Simplified formulations for two-dimensional TE-polarization field computations," in *IEEE Trans. Antannas and Propagat.* , vol. AP-39, pp. 259-262, Feb., 1991.

2. Kefeng Liu, C. A. Balanis and G. C. Barber, "Exact mutual impedance between sinusoidal electric and magnetic dipoles," in *IEEE Trans. on Antennas and Propogat.*, vol. AP-39, pp. 684-686, May, 1991.

3. Kefeng Liu, C. A. Balanis and G. C. Barber, "Low-loss material coating for horn antenna beam shaping," in *IEEE AP-S International Symposium Digest* (London, Ontario, Canada), vol. 3, pp. 1664-1667, June 1991.

References

[1] M. Burton and S. Kashyap, "Using software to push back the limits of the moment method," *IEEE Antennas Propagat. Soc. Int. Symp. Dig.*, vol. 3, London, Ontario, Canada, pp. 1504–1507, June 1991.

[2] J. T. Williams, H. J. Delgado, and S. A. Long, "An antenna pattern measurement technique for eliminating the fields scattered from the edges of a finite ground plane," *IEEE Trans. Antennas Propagat.*, vol. AP-38, pp. 1815–1822, Nov. 1990.